Stress Field Around Interface Free Edge of Elastic/Elastic-Plastic Material Joints

Samadder Liton KUMAR*, Yoshio ARAI** and Eiichiro TSUCHIDA**

* *Graduate Student of Saitama University, Saitama*
** *Department of Mechanical Engineering, Saitama University, Saitama*

Characteristics of singular stress field around an interface free edge between elastic and elastic-plastic materials, especially for the ceramic/metal joints with a interlayer were investigated theoretically. Finite element simulations have also been conducted to accomplish the quantitative examinations of the theoretical results. Elastic/linear hardening predictions and elastic/power-law hardening predictions were considered in the analysis. The simulation results of stress distribution clearly showed that the singular fields exist around the interface free edge between the elastic and elastic-plastic materials. Variables separable form functions of stress distribution were examined around the interface free edge. The availability of the elastic/linear hardening materials interface edge prediction was discussed.

1. INTRODUCTION

Many engineering structures comprise elastic or elastic-plastic materials. For strength evaluations of such structures as ceramic/metal joints, it is important to clarify characteristics of singular stress fields around an interface free edge of the joints[1 - 8]. Analytical studies on the stress singularity around the interface free edge of elastic/elastic-plastic materials joint have been conducted by many researchers. Duva, Rahman and Reedy modelized the elastic/power-law hardening plastic materials joint as a power-law hardening plastic material on a rigid substrate[9 - 13]. They conducted the asymptotic analysis similar to the nonlinear crack problem developed by Hutchinson[14 - 16]. Xu et al. and Arai et al. independently proposed the analogy between of the linear hardening materials joint and elastic materials joint[17 - 21]. The stress fields around the interface free edge can be expressed by $r^{\lambda-1}$ for a power-law hardening/rigid materials joint and a power-law hardening materials joint which have the same power index, n[22), 23)], where r is the distance from the interface edge and λ is the eigen value. Linear hardening materials joint can be a special case when the power $n = 1$ in the latter joint. In many cases ceramic/metal joints which are joined at some elevated temperature have an interlayer between the ceramics and the metal to reduce thermal residual stresses. When a power-law hardening material like copper is used as the interlayer, the material combination between the ceramics and the interlayer results in elastic and power-law hardening materials. The continuity of displacement and the equilibrium of force on the interface conflicts the dominance of a separable form singular solution like $u_i \propto r^{\lambda} f_i(\theta)$ for the material combination where u_i is the displacement component and $f_i(\theta)$ is the angular function. Applicability of the power-law/rigid materials joint model to ceramic/metal joints in regard to the interface free edge problem should be examined quantitatively. However the quantitative simulation based on the experimental results of the characteristics of stress singularity in ceramic/metal joints especially focusing on the existence of separable form distribution and the availability of linear hardening approximation in the ceramic side have not been presented.

In this study characteristics of singular fields around an interface free edge between elastic and elastic-plastic material joint, especially for the ceramic/metal joints with a interlayer were investigated theoretically. Finite element simulations have also been conducted to accomplish the quantitative examinations with the theoretical results. Elastic/linear hardening materials interface edge predictions and elastic/power-law hardening materials interface edge predictions were considered in the analysis. The simulation results of stress distribution clearly showed that the singular fields exist around the interface free edge between the elastic and elastic-plastic materials. Separable form functions of stress distribution were examined around the interface free edge. The availability of the elastic/linear hardening materials interface edge prediction was discussed.

2. ANALITICAL PROCEDURES

Consider a joint plate shown in Fig. 1(a) which is subjected to bending stress at $y = -L - 2t$ with the maximum bending stress $\sigma_y = p_0 (\sigma_y = \frac{p_0}{W}(W - x), \tau_{yx} = 0$ at $y = -L - 2t)$ and $u_y = 0$, $\tau_{yx} = 0$ at $y = L$. Around an interface free edge, O, in Fig. 1 (a) the continuity of displacement on the interface, the equilibrium of force on the interface and the stress free condition on the free edge are expressed as follows:

$$(u_i^I)_{\theta=0^\circ} = (u_i^{II})_{\theta=0^\circ}, \tag{1}$$

$$(\sigma_{ij}^I)_{\theta=0^\circ} = (\sigma_{ij}^{II})_{\theta=0^\circ}, \tag{2}$$

$$(\sigma_{ij}^I)_{\theta=90^\circ} = (\sigma_{ij}^{II})_{\theta=-90^\circ} = 0, \tag{3}$$

where, $i = r$ or θ, $ij = \theta\theta$ or θr, σ_{ij} denotes stress component. The stresses, displacements and material properties of the material 1 are referred to with a superscript "I"(e. g., σ_{rr}^I, ε_{rr}^I, ν^I, etc), while those of the material 2, with a superscript "II"(σ_{rr}^{II}, ε_{rr}^{II}, ν^{II}, etc).

2.1 Elastic singularity

The near interface free edge stress fields for the joint plate in elastic stress state can be expressed as follows[2 - 6), 20), 21)]:

$$u_i^m = p_0 k \left(\frac{r}{t}\right)^{\lambda} \bar{u}_i^m(\theta; \lambda), \tag{4}$$

$$\sigma_{ij}^m = p_0 k \left(\frac{r}{t}\right)^{\lambda - 1} F_{ij}^m(\theta; \lambda), \tag{5}$$

where λ is an eigen value, t is a characteristic length of the joined plates in this large aspect ratio[20)], k is a stress intensity factor with t, and $F_{ij}^m(\theta; \lambda)$ is determined by $F_{\theta\theta}^m(\theta = 0; \lambda) = 1$[6)], $\bar{u}_i^m(\theta; \lambda)$ is the angular function for the displacement component, u_i^m.

The eigenvalues, λ, is a root of the following equation:

$$\begin{aligned} &\lambda^2(\lambda^2 - 1)\alpha^2 + 2\lambda^2[\sin^2(\tfrac{\pi\lambda}{2}) - \lambda^2]\alpha\beta \\ &+[\sin^2(\tfrac{\pi\lambda}{2}) - \lambda^2]^2\beta^2 + \sin^2(\tfrac{\pi\lambda}{2})\cos^2(\tfrac{\pi\lambda}{2}) = 0, \end{aligned} \tag{6}$$

where α and β are Dundurs's composite parameters[24)],

$$\alpha = \frac{\Gamma(\kappa^I + 1) - (\kappa^{II} + 1)}{\Gamma(\kappa^I + 1) + \kappa^{II} + 1}, \tag{7}$$

$$\beta = \frac{\Gamma(\kappa^I - 1) - (\kappa^{II} - 1)}{\Gamma(\kappa^I + 1) + \kappa^{II} + 1}, \tag{8}$$

where $\Gamma = \frac{G^{II}}{G^I}$, G^m and ν^m are shear modulus and Poisson's ratio, respectively, κ^m is $3 - 4\nu^m$ for plane strain and $\frac{3-\nu^m}{1+\nu^m}$ for plane stress.

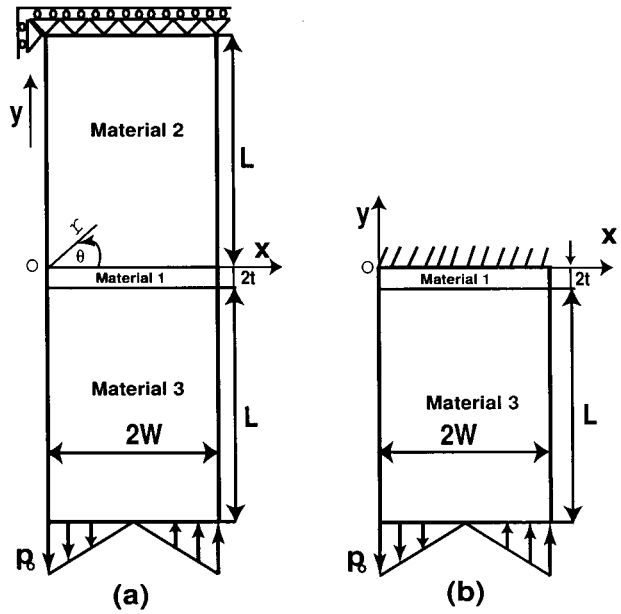

Fig. 1 (a) Elastic-plastic (material 1) and elastic (material 2) materials joint, (b) elastic-plastic material (material 1) bonded to rigid substrate, subjected to remote bending.

2.2 Singularity around an interface free edge of linear hardening elastic-plastic materials

According to the deformation theory, the stress-strain relations for linear hardening materials are given by the following equations[26]:

$$\varepsilon_{ij}^m = \frac{1}{E^m}\left\{(1+\nu^m)\sigma_{ij}^m - \nu^m\sigma_{kk}^m\delta_{ij}\right\} + \omega^m(1-\rho)\frac{s_{ij}^m}{E^m}, \tag{9}$$

$$s_{ij}^m = \sigma_{ij}^m - \frac{1}{3}\sigma_{kk}^m\delta_{ij}, \tag{10}$$

where ω^m is a hardening constant, ρ is unity before yielding and zero after yielding, s_{ij}^m is the deviatoric stress, E^m is the Young's modulus. A summation convention on the subscripts is assumed. By comparing the elastic and linear hardening constitutive equations for plane stress or plane strain conditions, it is apparent that the solution of the linear hardening problem is equivalent to the solution of the elastic problem[14], with the elastic properties, ν^m and Γ replaced by $\bar{\nu}^m$ and $\bar{\Gamma}$, defined below,

$$\bar{\nu}^m = \frac{\nu^m + \frac{1}{3}\omega^m}{1+\frac{2}{3}\omega^m}, \tag{11}$$

$$\bar{\Gamma} = \Gamma\left(\frac{1+\frac{\omega^I}{1+\nu^I}}{1+\frac{\omega^{II}}{1+\nu^{II}}}\right). \tag{12}$$

The index of the singularity for the linear hardening materials joint can be calculated from equations (6), (7) and (8) with the elastic properties, ν^m and Γ replaced by $\bar{\nu}^m$ and $\bar{\Gamma}$. When the material 2 is elastic, we can set $\omega^{II} = 0$. If we set $\omega^I \to \infty$, low hardening material (material 1) is perfectly plastic. In this case, if we set $\bar{\nu}^I = 0.5$ and $\bar{\Gamma} \to \infty$, then we have $\lambda \to 0.595$. When the material 2 is rigid, we set $\bar{\Gamma} \to \infty$. In this case, if we set $\nu^I = 0.3$, $\alpha = 1.0$ and $\beta = 0.2857$, then we have $\lambda = 0.71$.

2.3 Singularity around an interface free edge of power-law hardening elastic-plastic materials

According to the deformation theory, the stress-strain relations for power-law hardening materials are given by following equations[14]:

$$\frac{\varepsilon_{ij}^m}{\varepsilon_0} = (1+\nu^m)\frac{\sigma_{ij}^m}{\sigma_0} - \nu^m \frac{\sigma_{kk}^m}{\sigma_0}\delta_{ij} + \frac{3}{2}\alpha^m \left(\frac{\sigma_e^m}{\sigma_0}\right)^{n^m-1} \frac{s_{ij}^m}{\sigma_0}, \tag{13}$$

$$\sigma_e^m = \sqrt{\frac{3}{2} s_{ij}^m s_{ij}^m}, \tag{14}$$

where $(\sigma_0, \varepsilon_0)$ is a reference point in the stress-strain relation.

According to Hutchinson's asymptotic nonlinear crack solution in homogeneous material[14], we introduce an Airy stress function as follows:

$$\phi^m = A^m r^{\lambda^m+1} f^m(\theta) + \hat{\phi}^m(r,\theta), \tag{15}$$

where A^m is a constant, $f^m(\theta)$ is an angular function and $\hat{\phi}^m(r,\theta)$ is a higher order or non-variable separable function of r and θ. From the Airy stress function the following expressions for displacements and stresses are derived[27]:

$$u_i^m = r^{n^m(\lambda^m-1)+1}\bar{u}_i^m(\theta) + \hat{u}_i^m(r,\theta), \tag{16}$$

$$\sigma_{ij}^m = r^{\lambda^m-1}\bar{\sigma}_{ij}^m(\theta) + \hat{\sigma}_{ij}^m(r,\theta), \tag{17}$$

where $\hat{u}_i^m(r,\theta)$ and $\hat{\sigma}_{ij}^m(r,\theta)$ are the higher order or non-variable separable functions of r and θ for displacement and stress. The continuity conditions of displacement and the equilibrium of force on the interface between the power-law hardening materials with different power index, n^I and n^{II}, can be expressed as follows:

$$r^{n^I(\lambda^I-1)+1}\bar{u}_i^I(\theta=0) + \hat{u}_i^I(r,\theta=0) = r^{n^{II}(\lambda^{II}-1)+1}\bar{u}_i^{II}(\theta=0) + \hat{u}_i^{II}(r,\theta=0), \tag{18}$$

$$r^{\lambda^I-1}\bar{\sigma}_{ij}^I(\theta=0) + \hat{\sigma}_{ij}^I(r,\theta=0) = r^{\lambda^{II}-1}\bar{\sigma}_{ij}^{II}(\theta=0) + \hat{\sigma}_{ij}^{II}(r,\theta=0). \tag{19}$$

If material 2 is elastic, n^{II} is set to be 1. When $r \to 0$, i. e., the variable separable form functions are dominant, it is impossible to satisfy both conditions of the continuity of displacement and the equilibrium of force on the interface because the power of r in the displacement continuity (equation (18)) depends on the material constants, n^I and n^{II}, but the one in the equilibrium of force (equation (19)) does not.

In this paper, the following special cases are examined:

Case (1) $\lambda^I = \lambda^{II} = \lambda$.

Case (2) $n^I(\lambda^I - 1) = n^{II}(\lambda^{II} - 1)$.

Case (1) means the power of r for the variable separable function of stresses is common to that of the joined materials (material 1 and 2).

$$u_i^m = r^{n^m(\lambda-1)+1}\bar{u}_i^m(\theta) + \hat{u}_i^m(r,\theta), \tag{20}$$

$$\sigma_{ij}^m = r^{\lambda-1}\bar{\sigma}_{ij}^m(\theta) + \hat{\sigma}_{ij}^m(r,\theta). \tag{21}$$

In this case, the conditions of the continuity of displacement and the equilibrium of force on the interface between the power-law hardening materials with different n^m can be expressed as follows:

$$r^{n^I(\lambda-1)+1}\bar{u}_i^I(\theta=0) + \hat{u}_i^I(r,\theta=0) = r^{n^{II}(\lambda-1)+1}\bar{u}_i^{II}(\theta=0) + \hat{u}_i^{II}(r,\theta=0), \tag{22}$$

$$r^{\lambda-1}\bar{\sigma}_{ij}^I(\theta=0) + \hat{\sigma}_{ij}^I(r,\theta=0) = r^{\lambda-1}\bar{\sigma}_{ij}^{II}(\theta=0) + \hat{\sigma}_{ij}^{II}(r,\theta=0). \tag{23}$$

Assuming $\bar{u}_i^{II}(\theta=0) \neq 0$ and dividing the equation of displacement continuity by $r^{n^I(\lambda-1)+1}\bar{u}_i^{II}(\theta=0)$, we have the following equation:

$$\frac{\bar{u}_i^I(\theta=0)}{\bar{u}_i^{II}(\theta=0)} + r^{-n^I(\lambda-1)-1}\frac{\hat{u}_i^I(r,\theta=0)-\hat{u}_i^{II}(r,\theta=0)}{\bar{u}_i^{II}(\theta=0)} = r^{(n^{II}-n^I)(\lambda-1)}. \tag{24}$$

As the material 1 is assumed to be low hardening material, $n^{II}-n^I<0$. Existing a stress singularity gives $\lambda-1<0$ according to equation (21). Then $(n^{II}-n^I)(\lambda-1)>0$, the right-hand side of the above equation goes to zero when $r\to 0$. To ensure the continuity of displacement on the interface the left-hand side of equation (24) also should go to zero. However the first term does not depend on r so the term must be zero identically. This means that $\bar{u}_i^I(\theta=0)=0$ is a necessary condition for the continuity of displacement on the interface when $r\to 0$. The stress and displacement fields in the low hardening material (material 1) are controlled by the boundary condition which is the same as the one of an elastic-plastic material on the rigid substrate. The index of singularity, λ, can be determined using the boundary condition, $(u_i^I)_{\theta=0^\circ}=0$ and $(\sigma_{ij}^I)_{\theta=90^\circ}=0$. The stress field in the high hardening material (material 2) could also be controlled by the index through the equilibrium of force on the interface (equation (23)) when $r\to 0$. This formulation suggests that the index of singularity around the interface free edge between the elastic and elastic-plastic materials does not depend on the elastic properties of the elastic material (material 2).

Case (2) means the power of r in the variable separable form function of displacements is common to that of the joined materials (material 1 and 2). The conditions of the continuity of displacement and the equilibrium of force on the interface between the power-law hardening materials with different n^m can be expressed as follows:

$$r^{n^I(\lambda^I-1)+1}\bar{u}_i^I(\theta=0)+\hat{u}_i^I(r,\theta=0) = r^{n^{II}(\lambda^{II}-1)+1}\bar{u}_i^{II}(\theta=0)+\hat{u}_i^{II}(r,\theta=0), \tag{25}$$

$$r^{\lambda^I-1}\bar{\sigma}_{ij}^I(\theta=0)+\hat{\sigma}_{ij}^I(r,\theta=0) = r^{\lambda^{II}-1}\bar{\sigma}_{ij}^{II}(\theta=0)+\hat{\sigma}_{ij}^{II}(r,\theta=0). \tag{26}$$

Assuming $\bar{\sigma}_{ij}^{II}(\theta=0)\neq 0$, and dividing the equilibrium of force on the interface by $r^{\lambda^I-1}\bar{\sigma}_{ij}^{II}(\theta=0)$, we have the following equation:

$$\frac{\bar{\sigma}_{ij}^I(\theta=0)}{\bar{\sigma}_{ij}^{II}(\theta=0)} + r^{-\lambda^I+1}\frac{\hat{\sigma}_{ij}^I(r,\theta=0)-\hat{\sigma}_{ij}^{II}(r,\theta=0)}{\bar{\sigma}_{ij}^{II}(\theta=0)} = r^{\lambda^{II}-\lambda^I}. \tag{27}$$

From $n^I>n^{II}$ and $n^I(\lambda^I-1)=n^{II}(\lambda^{II}-1)$, it is obvious that $\lambda^{II}-\lambda^I>0$ gives the right-hand side of the equation (27) goes to zero when $r\to 0$. The similar discussion to Case (1) gives $\bar{\sigma}_{ij}^I(\theta=0)=0$ is a necessary condition for the equilibrium of force on the interface when $r\to 0$. This means that the stress and displacement fields in the low hardening material (material 1) should satisfy the condition of 90° apex with stress free edge condition. In Case (2) condition no singularity occurs.

The assumptions of Case (1) and Case (2) are examined by evaluating of stress and displacement fields obtained by the numerical calculations for a model material combination. The results of numerical calculations are compared to experimental results to verify the reliability.

2.4 NUMERICAL CALCULATIONS

The stress fields were calculated numerically by using elastoplastic finite element method. In Fig. 1, material 1 was assumed to be one of three material models, i. e., elastic; elastic linear-hardening plastic with yield strength, σ_{ys}^I, and hardening constant, ω^I; or elastic power-law hardening plastic with yield strength, σ_{ys}^I, and hardening constant, α^I and n^I. Material 2 was assumed to be elastic (Fig. 1 (a)) or rigid (Fig. 1 (b)). Plane strain 8 nodes isoparametric elements were used. As shown in Fig. 2, finite element meshes were divided into 30 in the near edge area, $0<r/t\leq 0.1$, along radial axis. The length of elements along radial axis varies as follows:

$$l_i = \frac{l_{i-1}}{0.9}, \qquad i=1,2,...30, \tag{28}$$

where l_i is a radial length of i-th element. The minimum length of elements, l_0/t, is 10^{-2}. For circumferential direction meshes are divided into 20 by equal angle. The total number of elements is 2044 and the total number of nodes is 6307.

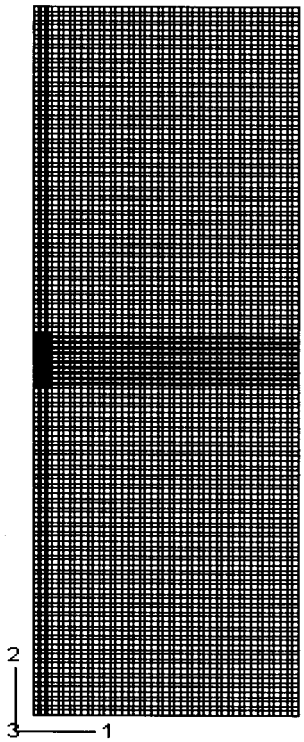

(a) Mesh division of whole model

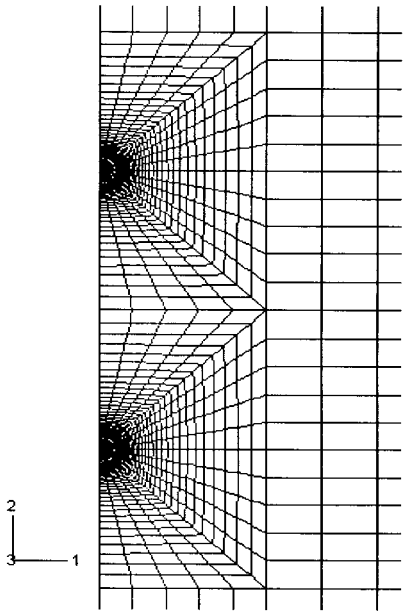

(b) Mesh division near interface edge

Fig. 2 Mesh division

Table 1 Mechanical properties of joined materials

(a) Elastic properties

(a-1) Si_3N_4/Cu/SUS304

	Material 1	Material 2	Material 3
E[GPa]	108	304	197
ν	0.33	0.27	0.30

(a-2) $Si_3N_4\times10$/Cu/SUS304 or $Si_3N_4\times100$/Cu/SUS304

	Material 1	Material 2	Material 3
E[GPa]	108	3040 or 30400	197
ν	0.33	0.27	0.30

(b) Plastic properties of material 1

(b-1) Power-law hardening

σ_{ys}^I [MPa]	50
n^I	2.4
α^I	10.1

(b-2) Linear hardening law

σ_{ys}^{I} [MPa]	50
ω^{I}	231

The model joint calculated in this study is a ceramic/metal joint with an interlayer such that Si_3N_4 as the ceramic, SUS304 as the metal and Cu as the interlayer[28].

The joint was selected for the comparison of our numerical results to the experimental results obtained by a laser moiré interferometry. The mechanical properties of each materials are listed in Table 1 and the hardening property of Cu experimentally measured is shown in Fig. 3 as well as the relations modelized by the power-law and linear hardening law. The dimensions of the model joint were $2W = 3$mm, $L = 5$mm and $2t = 0.4$mm. The external bending stress was $\sigma = 273$MPa which is large enough to develop a fully plastic zone in the elastic-plastic material. As listed in Table 1 (a-2) ideal material combination (the Young's modulus of material 2 is 10 or 100 times the one of Si_3N_4) were also calculated and the results were discussed.

3. RESULTS AND DISCUSSIONS

The distribution of displacement components, u_r and u_θ, along the θ direction when $r = 0.001$mm is shown in Fig. 4. The amplitude of displacement distribution along θ in the elastic material ($\theta > 0$, material 2) is significantly small compared with the one in the elastic-plastic material ($\theta < 0$, material 1). From the displacement distribution in Fig. 4 one can confirm the logical result of the Case (1) which insists the displacement fields in the low hardening material (material 1) approach to the one in the elastic-plastic material on the rigid substrate when $r \to 0$.

Table 2 Comparison of index of singularity, λ.

Elastic /elastic	0.92					
Elastic /linear hardening($\Gamma \to \infty$)	0.71					
Elastic /linear hardening($\omega^I \to \infty$)	0.60					
Rigid/power-law hardening (Duva)	0.76					
Rigid/power-law hardening (Rahman et al.)	0.75					
	Si_3N_4/Cu/SUS304			Rigid/Cu/SUS304		
θ (deg.)	90°	0°	-90°	-90°		
σ_r	0.76	0.76	0.75	0.75		
u_r	-	-	-	0.76		
u_θ	-	-	-	0.74		
θ (deg.)	45°	0°	-45°	-45°		
σ_θ	0.73	0.72	0.70	0.70		
$\tau_{r\theta}$	0.73	0.75	0.70	0.70		
	Si_3N_4×10/Cu/SUS304			Si_3N_4×100/Cu/SUS304		
θ (deg.)	90°	0°	-90°	90°	0°	-90°
σ_r	0.76	0.76	0.73	0.76	0.76	0.73
θ (deg.)	45°	0°	-45°	45°	0°	-45°
σ_θ	0.73	0.72	0.70	0.73	0.72	0.70
$\tau_{r\theta}$	0.73	0.75	0.70	0.73	0.75	0.72

The distribution of stress components, σ_{rr}, $\sigma_{\theta\theta}$ and $\sigma_{r\theta}$, along the r direction are shown in Fig. 5, 6 and 7, respectively. The slopes of log - log plot seem to be identical for all stress components when $r \to 0$ ($r < 10^{-2}$ mm) regardless of θ. These results imply that the power of r for the separable function of stresses is common to that of the joined materials which is the assumption of Case (1). The magnitude of the slope of finite element results for Si_3N_4/Cu/SUS304 joint is almost the same as the one for Rigid/Cu/SUS304 joint. The stress field in the more hardening material ($\theta = 89°$, material 2) is also controlled by the index

of singularity for the rigid/elastic-plastic material interface free edge through the equilibrium of force on the interface as discussed in Case (1) of section 2.3. Two predictions based on the linear hardening theory, the case of perfectly plastic material 1 ($\omega^I \rightarrow$Infinity) and the case of the rigid material 2 ($\Gamma \rightarrow$Infinity) give reasonable values of slope compared to the finite element simulations. These prediction methods using equation (6) - (8), (11) and (12) are valid and more convenient than the time consuming numerical elasto-plastic calculations.

The index of the stress singularity, λ, obtained by the numerical simulations as well as the linear hardening theory and the nonlinear asymptotic solution(after Duva and Rahman et al.[9), 11)]) are listed in Table 2. λ for the elastic/elastic-plastic materials joint by the present study ("Si_3N_4/Cu/SUS304" in the table) agree well with the one of the rigid/elastic-plastic materials joint by the finite element results("Rigid/Cu/SUS304" in the table) and the reference results ("Duva" and "Rahman et al." in the table).

These results imply that the stress and displacement fields around the interface free edge of the elastic/elastic-plastic materials joint can be described by the singular fields of an elastic-plastic material on the rigid substrate. The index of singularity, λ, can be determined using the boundary condition $(u_i^I)_{\theta=0^\circ} = 0$ and $(\sigma_{ij}^I)_{\theta=90^\circ} = 0$. Calculated λ by the finite element results("Rigid/Cu/SUS304" in the table) reproduced the nonlinear asymptotic solution(after Duva and Rahman et al.) which ensure the numerical accuracy of the present study. The index of the stress singularity for the elastic/elastic-plastic materials joint is smaller than the one in case of the elastic analysis ("Elastic/elastic" in the table).

Table 3 Variations of normalized stress distribution along θ direction (Si_3N_4/Cu/SUS304).

	Power law hardening			Linear hardening		
	σ_r	σ_θ	$\tau_{r\theta}$	σ_r	σ_θ	$\tau_{r\theta}$
Elastic %	2	4	9	10	8	18
E-P %	12	8	22	12	3	31

The smaller λ gives larger stress concentrations similar to the one generated by cracks ($\lambda = 0.5$). "$Si_3N_4 \times$ 10/Cu/SUS304" and "$Si_3N_4 \times$ 100/Cu/SUS304" in the table listed the results when the Young's modulus of the elastic material (material 2) is 10 times or 100 times the value of Si_3N_4. These results demonstrate that the index of singularity does not depend on the Young's modulus of the elastic material joined with the elastic-plastic material.

The distribution of stress components, σ_{rr}, $\sigma_{\theta\theta}$ and $\sigma_{r\theta}$, along the θ direction at various points of r is shown in Fig. 8, 9 and 10. The stress values are normalized by the maximum value or the value on the interface. The normalized distributions of stresses at various r lie on almost identical curve, which means the separable form distribution is dominant for the r range ($0.01 \leq r \leq 0.1$)mm. The linear hardening prediction ($\omega^I = 231$, bold line) shows better agreement with the numerical results than the distribution based on the elastic analysis (thin line). The maximum variation in percentage of each distribution of normalized stresses at various r are listed in Table 3. The variations in the elastic material side of the elastic/elastic-plastic materials joint are smaller than the one in the elastic-plastic material.

The comparison of stress distribution along r direction in the elastic material side ($\theta = 90°$) for Si_3N_4/Cu/SUS304 joint between experimental results and numerical results is shown in Fig. 11[28]. The present numerical simulations ("Linear hardening, $\omega = 231$" and "Power-law hardening, n = 2.40" in Fig. 11) give reasonable agreement with the experimentally measured stress distribution. This result ensures that the stress concentration near the interface free edge of model joint (Si_3N_4/Cu/SUS304) calculated in this study is a realistic phenomena in the engineering applications.

The experimentally measured slope values of the log u_y - log y relations, λ (see equation (4)), was close to unity in the region far from the Si_3N_4/Cu interface and decreased with decreasing y at the external stress of 273MPa as shown in Fig. 12. The λ approached to a value between 0.6~0.7 in $y \leq 0.1$mm. This magnitude of λ was smaller than the one for the elastic/elastic materials interface edge("Elastic Prediction" in Fig. 12). The elastic/linear hardening material interface theory ("Linear hardening, $\omega = 231$" in Fig. 12) and the power-law hardening/rigid material interface theory("Power-law, n=2.40" in Fig. 12) can predict smaller λ compared with the elastic material interface theory.

It is supposed that the high stress concentration around the Si_3N_4/Cu interface free edge is due to the difference in the effective stiffness of the plastically deforming Cu and the elastic Si_3N_4. Two predictions are based on the state in which the plastic strain is dominant, while the finite element results of λ are depending on the distance from the interface, y.

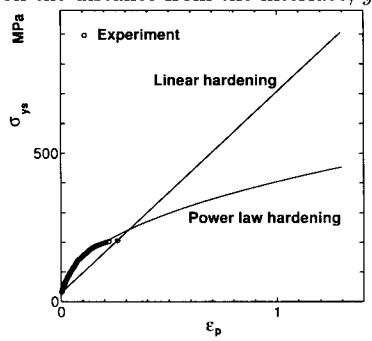

Fig. 3 Yield stress and plastic strain relationships during hardening (Cu)

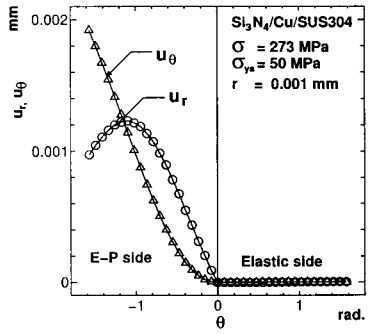

Fig. 4 Displacement distribution along θ near interface free edge of elastic/elastic-plastic materials

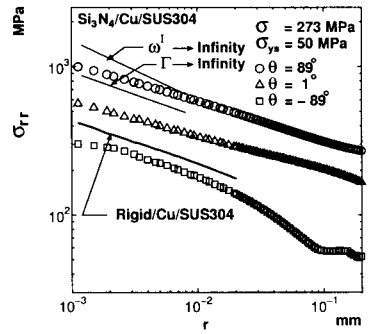

Fig. 5 $\log - \log$ plot of $\sigma_{\rm rr}$ distribution along r in elastic/elastic-plastic materials joint.

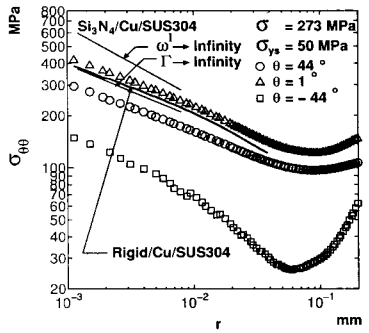

Fig. 6 $\log - \log$ plot of $\sigma_{\theta\theta}$ distribution along r in elastic/elastic-plastic materials joint.

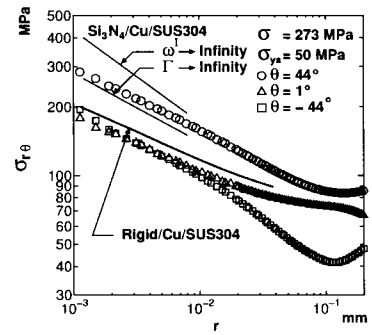

Fig. 7 $\log - \log$ plot of $\sigma_{r\theta}$ distribution along r in elastic/elastic-plastic materials joint.

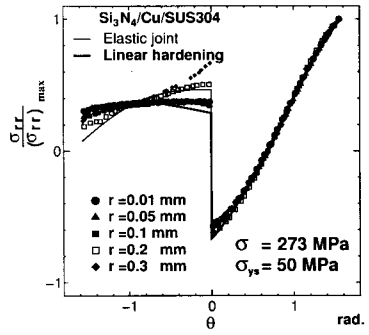

Fig. 8 Comparison of $\sigma_{\rm rr}$ distribution along θ at various points of r normalized by maximum value in elastic/elastic-plastic materials joint.

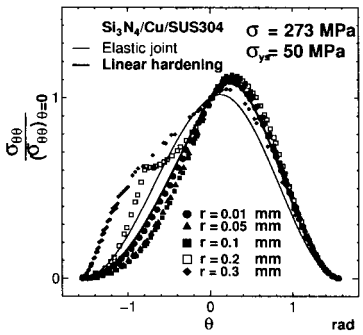

Fig. 9 Comparison of $\sigma_{\theta\theta}$ distribution along θ at various points of r normalized by interface value in elastic/elastic-plastic materials joint.

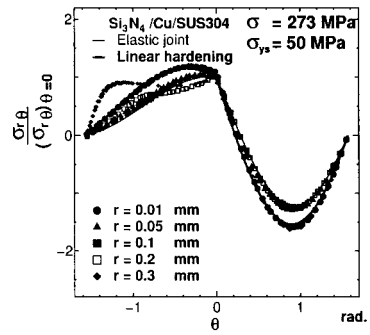

Fig. 10 Comparison of $\sigma_{r\theta}$ distribution along θ at various points of r normalized by interface value in elastic/elastic-plastic materials joint.

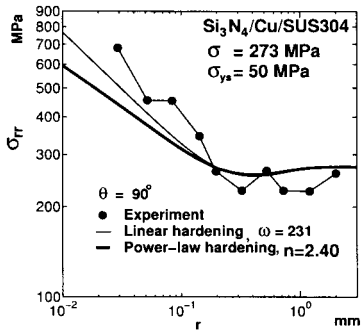

Fig. 11 Comparison of σ_{rr} distribution along r between experimental results ($\theta = 90°$) and calculated results ($\theta = 89°$).

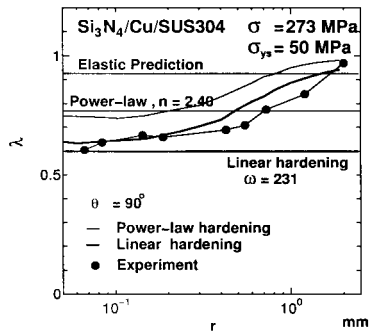

Fig. 12 Comparison of λ along θ ($\theta = 90°$) between experimental results and calculated results ($\theta = 89°$).

4. CONCLUSIONS

(1) The angular function of separable form term in the displacement fields should be zero at $\theta = 0$ is a necessary condition for the continuity of displacement on the interface when $r \to 0$ around the interface free edge of the elastic/elastic-plastic materials. The stress and displacement fields in the elastic-plastic material are controlled by the boundary condition which is the same as the one of an elastic-plastic material on the rigid substrate. The stress fields in the elastic material are also controlled by the index through the equilibrium of force on the interface.

(2) The index of singularity around the interface free edge of the elastic/elastic-plastic materials joint does not depend on the elastic properties of the elastic material.

(3) The slope of the log - log plot between the displacement u_y and the coordinate y in Si_3N_4 side far from the Si_3N_4/Cu interface approached to unity which is the slope in the homogeneous case. The slope decreased with decreasing the coordinate y in the log u_y - log y relations. The slope was in between $\lambda = 0.6$ and $\lambda = 0.7$ for $y \leq 0.2$mm. This slope is smaller than the predicted value using elastic/elastic materials interface edge theory which is calculated from the elastic modulus of Si_3N_4 and Cu.

(4) The linear hardening interface theory and the power-law hardening/rigid interface theory can predict the smaller λ compared with the elastic interface theory. It is supposed that the high stress concentration around the Si_3N_4/Cu interface edge is due to the difference in the effective stiffness of the plastically deforming Cu and the elastic Si_3N_4.

REFERENCES

1) Ruhle, M., Evans, A. G., Ashby, M. F. and Hirth, J. P., Ed., "Metal - Ceramic Interfaces," Acta metall. Proc. Ser., Vol. 4, Pergamon Press, 1989.
2) Williams, M. L., "The Stress Singularities Resulting From Various Boundary Conditions in Angular Corners of Plates in Extension," J. Appl. Mech., Vol. 19, pp. 526-529, 1952.
3) Bogy, D. B., "Edge-Bonded Dissimilar Orthogonal Elastic Wedges Under Normal and Shear Loading," ASME J. Appl. Mech., Vol. 35, pp.460-466, 1968.
4) Dempsey, J. P. and Sinclair, G. B., "On the singular behavior at the vertex of a bi-material wedge," J. Elasticity, Vol. 11, No. 3, pp. 317 - 327, 1981.
5) Blanchard, J. P. and Ghoniem, N. M., "An Eigenfunction Approach to Singular Thermal Stresses in Bonded Strip," J. Thermal Stresses, Vol. 12, pp.501-527, 1989. 6) Munz, D. and Yang, Y. Y., "Stress Singularities at the Interface in Bonded Dissimilar Materials Under Mechanical and Thermal Loading", J. Appl. Mech., Vol. 59, Dec., Trans. ASME, pp. 857 - 861, 1992.
7) Cao, H. C., Thouless, M. D. and Evans A. G., "Residual Stresses and Cracking in Brittle Solids Bonded with a Thin Ductile Layer," Acta metall. mater., Vol. 36, No. 8, pp. 2037 - 2046, 1988.
8) Post, D., Wood, J. D., Han, B, Parks, V. J. and Gerstle, F. P., "Thermal Stresses in a Bimaterial Joint: An Experimental Analysis," Trans. ASME, J. Appl. Mech., Vol. 61, pp. 192 - 198, 1994.
9) Duva, J. M., "The Singularity at the Apex of a Rigid Wedge Embedded in a Nonlinear Material," J. Appl. Mech. Vol. 55, pp. 361 - 364, 1988.
10) Duva, J. M., "The Singularity at the Apex of a Rigid Wedge After Partial Separation," J. Appl. Mech. Vol. 56, pp. 977 - 979, 1989.
11) Rahman, A., "Singular Stress Fields at Plastically Deforming Bimaterial Interfacial Notches and Free-Edges," Ph. D. Dissertation, Drexel University, Philadelphia, PA, 1991.
12) Rahman, A. and Lau, A. C. W., "Singular Stress Fields in interfacial notches of hybrid metal matrix composites," Composites Part B: Engineering, Volume 29, pp. 763 - 768, 1998.
13) Reedy, E. D., "Free-Edge Stress Intensity Factor for a Bonded Ductile Layer Subjected to Shear," J. Appl. Mech. Vol. 60, pp. 715 - 720, 1993.
14) Hutchinson, J. W., "Singular Behaviour at the End of a Tensile Crack in a Hardening Material," J. Mech. Phys. Solids, Vol. 16, pp. 13 - 31, 1968.
15) Shih, C. F. and Asaro, R. J., "Elastic-Plastic Analysis of Cracks on Bimaterial Interfaces: Part I Small Scale Yielding," ASME J. Appl. Mech., Vol. 55, pp.299-316, 1988.
16) Wang, T. C., "Elastic-Plastic Asymptotic Fields for Cracks on Bimaterial Interfaces," Engng. Fracture Mech., Vol. 37, No. 3, pp.527-538, 1990.
17) Xu, J.-Q. and Mutoh, Y., "Elastic Stress Singularity at Interface Edge with Arbitrary Bonding Angle in Dissimilar Linear Hardening Materials," Trans. JSME, Ser. A, Vol. 65, No. 630, pp. 277 - 281, 1999(in Japanese).
18) Xu, J.-Q., Fu, L.-D. and Mutoh, Y., "Elastic-Plastic Boundary Element Analysis of Interface Edge in Bonded Dissimilar Materials," J. Soc. Mat. Sci., Jpn., Vol. 49, No. 8, pp. 857 - 861, 2000(in Japanese).
19) Xu, J.-Q., Fu, L.-D. and Mutoh, Y., "A Method for Determining Elastic-Plastic Stress Singularity at the Interface Edge of Bonded Power Law Hardening Materials," JSME Int. J., Ser. A, Vol. 45, No. 2, pp. 177 - 183, 2002.
20) Arai, Y., Tsuchida, E. and Sakurai, T., "Study on Stress Field around Elastic/Elastic-Plastic Interface Edge," Theor. Appl. Mech., Vol. 49, pp. 33 - 39, 2000.
21) Arai, Y. and Tsuchida, E., "Dependence of Elastic-Plastic Stress Singularity Field on Material Combination of Butt-Jointed Plates Subjected Uniform Tension," Mater. Sci. Research Int., STP 1, pp. 233 - 237, 2001.
22) Lau, C. W., Rahman, A. and Delale, F., "Interfacial Mechanics of Seals," Technology of Glass, Ceramic, or Glass-Ceramic to Metal Sealing, W. E. Moddeman, et al., ed., ASME New York, MD-Vol. 4, pp. 89 - 98, 1987.
23) Lau, C. W. and Delale, F., "Interfacial Stress Singularities at Free Edge of Hybrid Metal Matrix Composites," J. Engng. Mater. Tech., Vol. 110, pp. 41 - 47, 1988.
24) Dundurs J., "Effect of Elastic Constants on Stress in a Composite under Plane Deformation," J. Composite Materials, Vol. 1, pp. 310 - 322, 1967.
25) Post, D., Han, B, Ifju, P., "High Sensitivity Moiré," Springer-Verlag, 1994.
26) Castaneda, P. P., "Asymptotic Fields in Steady Crack Growth with Linear Strain-Hardening," J. Mech. Phys. Solids, Vol. 35, No. 2, pp. 227 - 268, 1987.
27) Timoshenko, S. P. and Goodier, J. N., "Theory of Elasticity," Third edition, McGRAW-HILL, 1982.

28) Liton, S. K., Arai, Y., Tsuchida, E. and Yoshida, M., "Measurarement of Plane Strain Singular Field Around Interface Edge Using Moire Interferometery," Proc. SEM X International Congress & Exposition on Experimental and Applied Mechanics, 2004.